ASL deficiency in ALDH1A1^{+}- neurons in the substantia nigra metabolically promotes neurodegenerative phenotypes

Shaul Lerner[1], Raya Eilam[2], Lital Adler[1], Julien Baruteau[3,4], Topaz Kreiser[5], Michael Tsoory[2], Alexander Brandis[6], Tevie Mehlman[6], Mina Ryten[3,7], Juan A Botia[7,8], Sonia Garcia Ruiz[3,7], Alejandro Cisterna Garcia[8], Carlo Dionisi-Vici[9], Giusy Ranucci[9], Marco Spada[9], Ram Mazkereth[10], Robert McCarter[11,12], Rima Izem[11,12], Thomas J. Balmat[13], Rachel Richesson[14], "Members of the UCDC"[#], Ehud Gazit[5], Sandesh CS Nagamani[15, 16] and Ayelet Erez[1*]

[1]Department of Biological Regulation, Weizmann Institute of Science, Rehovot, Israel.

[2]Department of Veterinary Resources, Weizmann Institute of Science, Rehovot, Israel.

[3]Great Ormond Street Institute of Child Health, and NIHR Great Ormond Street Hospital Biomedical Research Centre, University College London, London, UK

[4]Great Ormond Street Hospital for Children NHS Foundation Trust, London, UK

[5]The Shmunis School of Biomedicine and Cancer Research, George S. Wise Faculty of Life Sciences, Tel Aviv University, Tel Aviv 6997801, Israel

[6]Life Science Core Facility, Weizmann Institute of Science, Rehovot, Israel.

[7]Institute of Neurology, University College London (UCL), London, UK

[8]Department of Information and Communications Engineering, University of Murcia, Spain

[9]Division of Metabolism, Bambino Gesù Children's Hospital IRCCS, Rome, Italy

[10]The Sackler School of Medicine, Tel-Aviv University, Tel-Aviv, Israel.

[11]Center for Translational Sciences, Children's National Health System, The George Washington University, Washington DC

[12]Children's National Medical Center, Washington, D.C.USA

[13] Research Computing, Duke University, Durham, NC, USA

[14] Learning Health Sciences, University of Michigan, Ann Arbor, MI, USA

[15]Department of Molecular and Human Genetics, Baylor College of Medicine, Houston, TX, USA.

[16]Texas Children's Hospital, Houston, TX, USA.

[#]Members of the UCDC are listed in the acknowledgements

[*]Corresponding author: Ayelet Erez MD, PhD; Weizmann Institute of Science, Rehovot, Israel; Phone- 972-8-934-3714; FAX- 972-8-934-3739; email: ayelet.erez@weizmann.ac.il

Abstract

Argininosuccinate lyase (ASL) is essential for the NO-dependent regulation of tyrosine hydroxylase (TH) and thus for catecholamine production. Using a conditional mouse model with loss of ASL in catecholamine neurons, we demonstrate that ASL is uniquely expressed in ALDH1A1^{+} subpopulation of dopaminergic neurons in the substantia nigra pars compacta, that are pivotal for the pathogenesis of Parkinson disease (PD). Neuronal loss of ASL results in catecholamine deficiency, in accumulation and formation of tyrosine aggregates, in elevation of α-synuclein, and phenotypically in motor and cognitive deficits. NO supplementation rescues the formation of aggregates as well as the motor deficiencies. We further report that 10% of individuals with ASLD manifest tremors and describe a locus in proximity to ASL that is associated with an increased risk for PD. Our data point to a potential metabolic link between accumulations of tyrosine and seeding of pathological aggregates in neurons as initiators for the pathological processes involved in neurodegeneration. Hence, interventions in tyrosine metabolism *via* regulation of NO levels may be therapeutic beneficial for the treatment of catecholamine-related neurodegenerative disorders.

Introduction

In the liver, the urea cycle enzymes argininosuccinate lyase (ASL) and argininosuccinate synthase 1 (ASS1) are required for the conversion of waste-nitrogen to urea. Loss of ASL or ASS1 activity causes argininosuccinic aciduria (or argininosuccinate lyase deficiency, ASLD, MIM#207900) and citrullinemia type 1 (MIM#215700), respectively. These two disorders are a subset of the classical inborn errors of metabolism called urea cycle disorders (UCD) that are characterized by episodes of hyperammonemia (Erez, Nagamani et al., 2011a, Kolker, Valayannopoulos et al., 2015b, Nagamani, Erez et al., 1993, Tuchman, Lee et al., 2008). In tissues other than the liver, ASL and ASS1 participate in the arginine-citrulline cycle, which generates arginine, an important metabolic nexus for the synthesis of essential metabolites such as creatine, proline, polyamines, glutamate, and nitric oxide (NO). While both ASL and ASS1 participate in the arginine-citrulline cycle, ASL is the only enzyme in mammals that is able to endogenously synthesize arginine (Erez, Nagamani et al., 2011b, Mori & Gotoh, 2004).

Individuals with germline pathogenic variants in *ASL* can have neurocognitive deficits, seizures, and motor abnormalities (Nagamani, Campeau et al., 2012). Whereas hyperammonemia is a major determinant for overall neurological outcomes in ASLD, some of the neurocognitive deficits and behavioral abnormalities have also been reported in individuals without significant hyperammonemia, suggesting, that they may be the result of a neuronal tissue-autonomous loss of ASL. We have recently reported that ASL deficiency in the locus coeruleus (LC), results in impaired NO synthesis, decreased tyrosine hydroxylase (TH) activity, and consequently, in low dopamine and norepinephrine levels (Lerner, Anderzhanova et al., 2019). Notably, both dopamine and norepinephrine are important neurotransmitters (Chrousos, 2009, Sara, 2009, Wise, 2004) and their deficiency has been associated with neurodegenerative disorders including PD (Miller & O'Callaghan, 2015, Schapira, Chaudhuri et al., 2017).

LC projects to the ventral tegmental area (VTA) and to the substantia nigra pars compacta (SNc). These projections are highly interconnected and are necessary for the survival of vulnerable midbrain dopaminergic neurons (Hassani, Rymar et al., 2020, Rommelfanger, Weinshenker et al., 2004, Srinivasan & Schmidt, 2003). Loss of these projections has been shown to facilitate neuronal degeneration and are responsible for some of the motor and non-motor symptoms associated with PD (Hassani et al., 2020, Kalia & Lang, 2015, Miller & O'Callaghan, 2015, Schapira et al., 2017). Specifically, within the SNc, there is a subpopulation of dopaminergic neurons that express aldehyde dehydrogenase, i.e., ALDH1A1^{+}-neurons. These neurons require ALDH1A1 for

their normal functioning and survival (Cai, Liu et al., 2014, Liu, Yu et al., 2014, Poulin, Zou et al., 2014); their preferential degeneration has been shown to contribute to the pathogenesis of PD and have been specifically implicated in movement impairments associated with PD (Galter, Buervenich et al., 2003, Wu, Kung et al., 2019). Furthermore, ALDHA1 levels in peripheral blood have been used as a biomarkers for PD (Grunblatt, Zehetmayer et al., 2010).

PD is characterized by impaired catecholamine levels as well as by the formation of amyloidogenic proteins and α-synuclein aggregates in SNc (Devine, Gwinn et al., 2011, Irwin, Lee et al., 2013). Interestingly, the key processes that are involved in the initiation and propagation of these protein aggregates remain elusive (Buxbaum & Linke, 2012, Dickson, 2018, Wong & Krainc, 2017); it has been suggested that accumulation of small metabolites act as "seeds" for the formation of the aggregates (Tavassoly, Sade et al., 2018). Based on these data from the literature, we hypothesized that decreased activity of ASL and TH would contribute to the pathogenesis of neurodegeneration by perturbing tyrosine metabolism.

Results

ASL is specifically expressed in TH - ALDH1A1^{+}- SNc neurons

By performing immunostaining in dopaminergic neurons in wild type mice, we found a distinctive pattern of expression for ASL that was specific for TH -ALDH1A1^{+}- SNc neurons (**Figure 1A and Supp. Figure 1A**). Conditional ASL knockout mice, i.e., *Asl$^{f/f}$;TH Cre$^{+/-}$* did not express ASL in this unique TH ALDH1A1^{+}sub-population of neurons (**Supp. Figure 1A**). Interestingly, these SNc-ALDH1A1^{+}neurons have been shown to undergo degeneration in PD and have been linked directly with the motor impairments associated with PD (Giguere, Burke Nanni et al., 2018, Liu et al., 2014). Using laser microdissection, we collected specific TH positive neurons from the SNc and VTA (**Supp. Figure 1B**). Corroborating our previous findings (Lerner et al., 2019), following *Asl* deletion (**Supp. Figure 1C**), we found reduction in *TH* mRNA levels in *Asl$^{f/f}$;TH Cre$^{+/-}$* mice as compared to control mice (*Asl$^{f/f}$*) (**Figure 1B**). Immunostaining of SNc- ALDH1A1^{+}neuronal sub-population demonstrated reduction in TH protein levels, specifically in the SNc of *Asl$^{f/f}$;TH Cre$^{+/-}$* as compared to control *Asl$^{f/f}$* mice (**Figure 1C and Supp. Figure 2A**). As SNc- ALDH1A1^{+}neurons are known to project predominantly to the dorsolateral striatum (Sgobio, Wu et al., 2017, Wu et al., 2019), we evaluated the expression of TH in ALDH1A1^{+} fibers in this region; we found that *Asl$^{f/f}$;TH Cre$^{+/-}$* mice show a significant reduction in TH levels in the striatum as well, in comparison to control mice (**Figure 1D**). To test whether the

downregulation of TH in dopaminergic neurons is functionally significant, we measured catecholamine levels in punch biopsies taken from the SNc region and found that *Asl*$^{f/f}$*;TH Cre*$^{+/-}$ have lower levels of dopamine and norepinephrine in comparison to *Asl*$^{f/f}$ control mice (**Figure 1E**). Additionally, cerebrospinal fluid (CSF) analysis from adult *Asl*$^{f/f}$*;TH Cre*$^{+/-}$ mice revealed elevated levels of ALDH1A1 protein in comparison to control mice (**Supp. Figure 2B**).

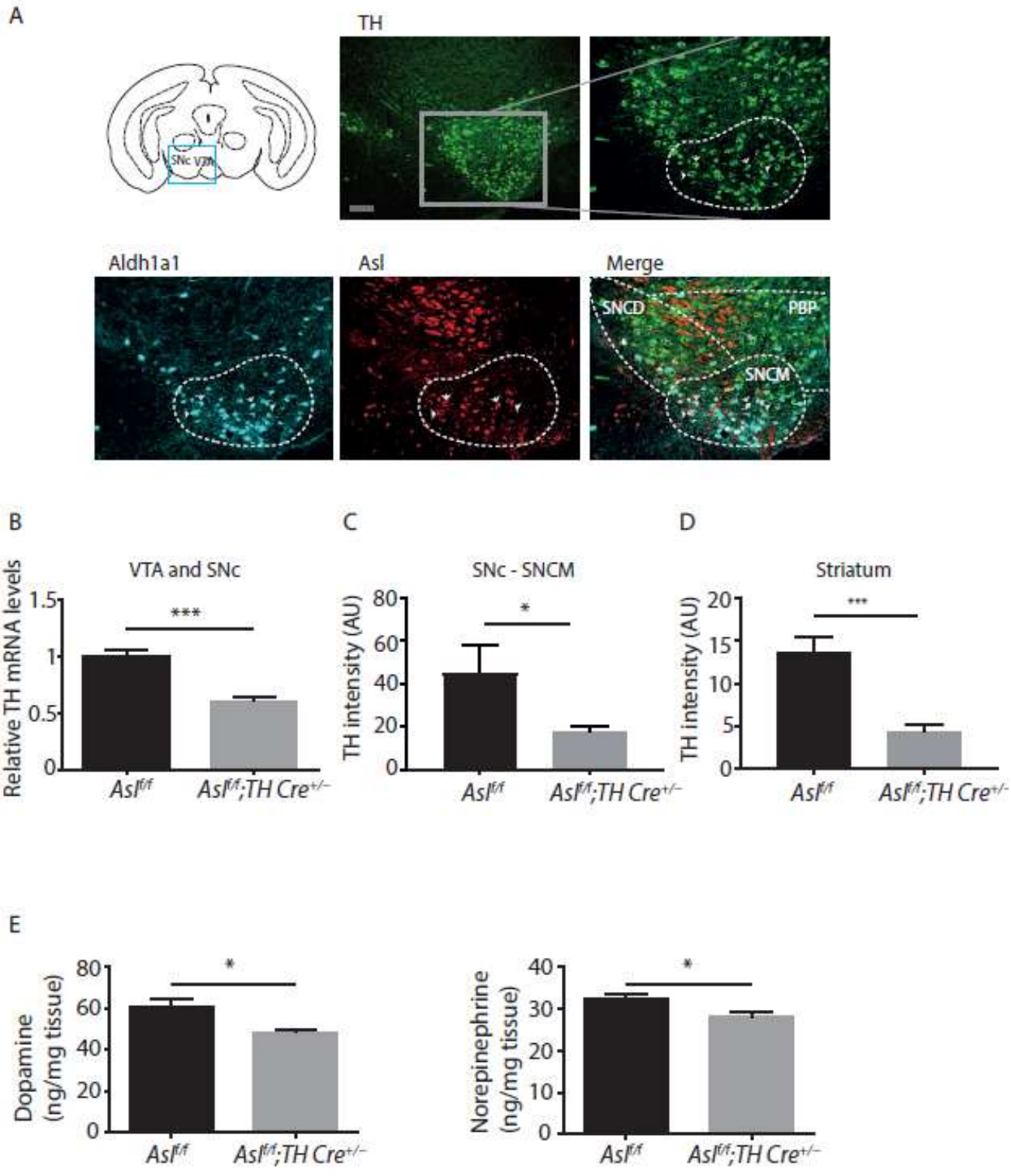

Figure 1: ASL co-localizes with TH and ALDH1A1in the SNc and its deficiency is associated with decreased TH expression and catecholamine synthesis.

(**A**) VTA and SNcM dopaminergic regions are demonstrated in a scheme of coronal midbrain section (bregma -3.65mm) (top panel left) and by TH staining (top panel middle, green) (Scale bar=500 µm). Magnification of the box area indicates TH (top panel right, green), ALDH1A1^{+} (lower panel left, cyan),

ASL (lower panel middle, red) and their co staining (lower panel right). Dashed lines differentiates the SNcM and VTA subregions (Scale bar=250 μm). Arrows point to representative cells co-expressing the three proteins. (**B**) Quantification of *TH* mRNA in the SNcM and VTA regions of *Asl$^{f/f}$;TH Cre$^{+/-}$* and in *Asl$^{f/f}$* control mice as measured by RT-PCR with specific TaqMan probes (n=7 mice in each group). (**C-D**) Quantification of TH immunostaining of TH- ALDH1A1^{+} neurons in the SNc medial (SNcM) (**C**) and striatum (**D**) of *Asl$^{f/f}$;TH Cre$^{+/-}$* and *Asl$^{f/f}$* control mice (n=5). (**E**) Measurement of SNcM catecholamine levels show reduction in both dopamine (left) and in norepinephrine (right) in *Asl$^{f/f}$;TH Cre$^{+/-}$* as compared to *Asl$^{f/f}$* control mice (n ≥ 9 mice in each group). SNCD-SNc dorsal, PBP-parabrachial pigmented nucleus. Data represent mean ± s.e.m. (*p < 0.05, **p < 0.01, ***p<0.001, ****p<0.0001; ns- not significant).

ASL deficiency is associated with motor deficits in mice with loss of ASL in TH - ALDH1A1^{+}- SNc neurons and in individuals with ASLD

The decreased catecholamine levels, specifically in the SNc region, led us to examine motor functions in *Asl$^{f/f}$;TH Cre$^{+/-}$* mice. Using gait pattern assessment test ("CatWalk^{TM} Gait Analysis" (Boix, von Hieber et al., 2018)), we found significant abnormalities in *Asl$^{f/f}$;TH Cre$^{+/-}$* mice in ten different gait parameters that are commonly found in rodent models of PD (Wang, Lu et al., 2012) (Boix et al., 2018) (**Figure 2A-H**). Multiple studies by us and others have shown that ASL is essential for NO generation and that ASL loss leads to NO-related pathologies including cognitive deficits (Erez et al., 2011b, Kho, Tian et al., 2018, Lerner et al., 2019, Nagamani et al., 2012, Stettner, Rosen et al., 2018). Specifically, in the context of catecholamine neurons, dysregulation of NO signaling has been shown to alter dopamine production (Lerner et al., 2019) (Harraz & Snyder, 2015). Hence, we next aimed to rescue the phenotypic consequences of ASL loss from dopaminergic neurons by supplementing *Asl$^{f/f}$;TH Cre$^{+/-}$* mice with NOS-independent NO donors. Encouragingly, adding NO supplement was sufficient to rescue many of the abnormal gait parameters (**Figure 2A-H**).

To evaluate whether our findings are relevant to humans with ASLD, we mined the clinical data collected by the NIH Rare Disease Clinical Research Network's Urea Cycle Disorders Consortium. We identified that a higher proportion of individuals with ASLD (23 out of 124, 18%) are reported to have tremors, as compared to individuals with ASS1D (5 out of 106, 5%) (p<0.05) (**Figure 2I**). Since hyperammonemia (HA) can be a confounder for many of the behavioral, cognitive and motor outcomes in UCDs, we further evaluated the prevalence of tremors in these two subsets of UCDs in individuals who did not have any documented episodes of HA. The percentage of individuals with ASLD and ASS1D without at least one documented episode of hyperammonemia were 42 (n=52) and 28 (n=29), respectively. In the absence of documented HA, the percentage of individuals with ASLD who had tremors was 19 (10 out of 52) as compared to 3 (1 out of 29) in ASS1D (**Figure 2I**).

Thus, the proportion of individuals with ASLD who reported tremors were higher as compared to ASS1D irrespective of history of presence or absence of documented hyperammonemia.

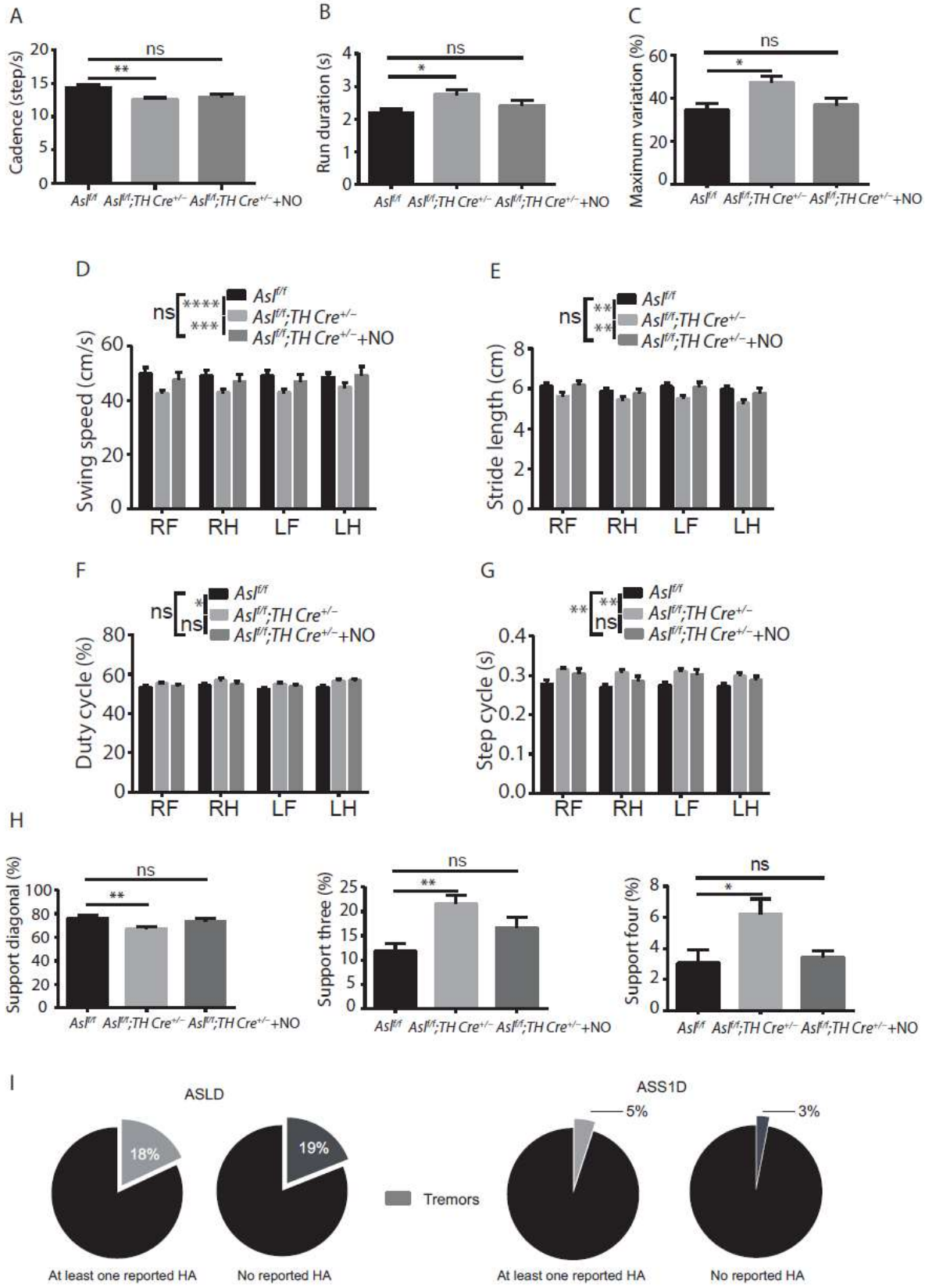

Figure 2: ASL deficiency in results in motor dysfunctions in both humans and rodents

(**A-H**) Gait analysis in *Asl$^{f/f}$;TH Cre$^{+/-}$* and *Asl$^{f/f}$* control mice. Dynamic paw parameters included (**A**) Cadence (**B**) Run duration (**C**) Maximum variation. (**D**) Swing speed. (**E**) Stride length (**F**) Duty cycle. (**G**) Step cycle. (**H**) Paws support. (n≥ 10). **(I)** Pie charts demonstrating the percentage of subjects with tremors in ASLD (left part) and ASS1D (right part) patients with or without documented episode of HA. Data represent mean ± s.e.m. (*p < 0.05, **p < 0.01, ***p<0.001, ****p<0.0001; ns- not significant).

Loss of ASL in TH - ALDH1A1^{+}- SNc neurons results in memory deficits

To evaluate the memory of *Asl$^{f/f}$;TH Cre$^{+/-}$* mice, we used Morris water maze (MWM) and the fear conditioning test (McDowell & Chesselet, 2012). In adult mice using the MWM test, we found that *Asl$^{f/f}$* control mice spent significantly more time in the target quarter as compared to *Asl$^{f/f}$;TH Cre$^{+/-}$*, while in younger mice, we did not observe any differences between the two genotypes (**Figure 3A, Supp. Figure 3A and data not shown**). Notably, across the 7 days of learning, all mice showed similar learning behavior, suggesting that although adult *Asl$^{f/f}$;TH Cre$^{+/-}$* are capable of learning, they have a problem in long-term memory consolidation (**Supp. Figure 3B**). To confirm these findings, we challenged the mice for a second time two weeks after the original probe day. Here again, adult *Asl$^{f/f}$;TH Cre$^{+/-}$* mice did not show preference for searching the platform in the target quarter, while the *Asl$^{f/f}$* control mice recalled the platform location (**Figure 3A**). Corroboratively, when we challenged adult *Asl$^{f/f}$;TH Cre$^{+/-}$* mice with the fear-conditioning paradigm for evaluating associative learning and memory, *Asl$^{f/f}$* control mice froze significantly more as compared to *Asl$^{f/f}$;TH Cre$^{+/-}$* mice in both context and cue tests (**Figure 3B**), a trend that remained even two weeks after the initial testing (**Figure 3C**). Together, these results imply that KO of ASL in catecholamine neurons of mice, decreases memory dependent performance.

To try and rescue these phenotypes, we supplemented the mice with NO donors for two weeks before the beginning of the experiments. Here, NO treatment significantly rescued *Asl$^{f/f}$;TH Cre$^{+/-}$* mice only in the fear-conditioning test and less so in the MWM test (**Figure 3A-C**).

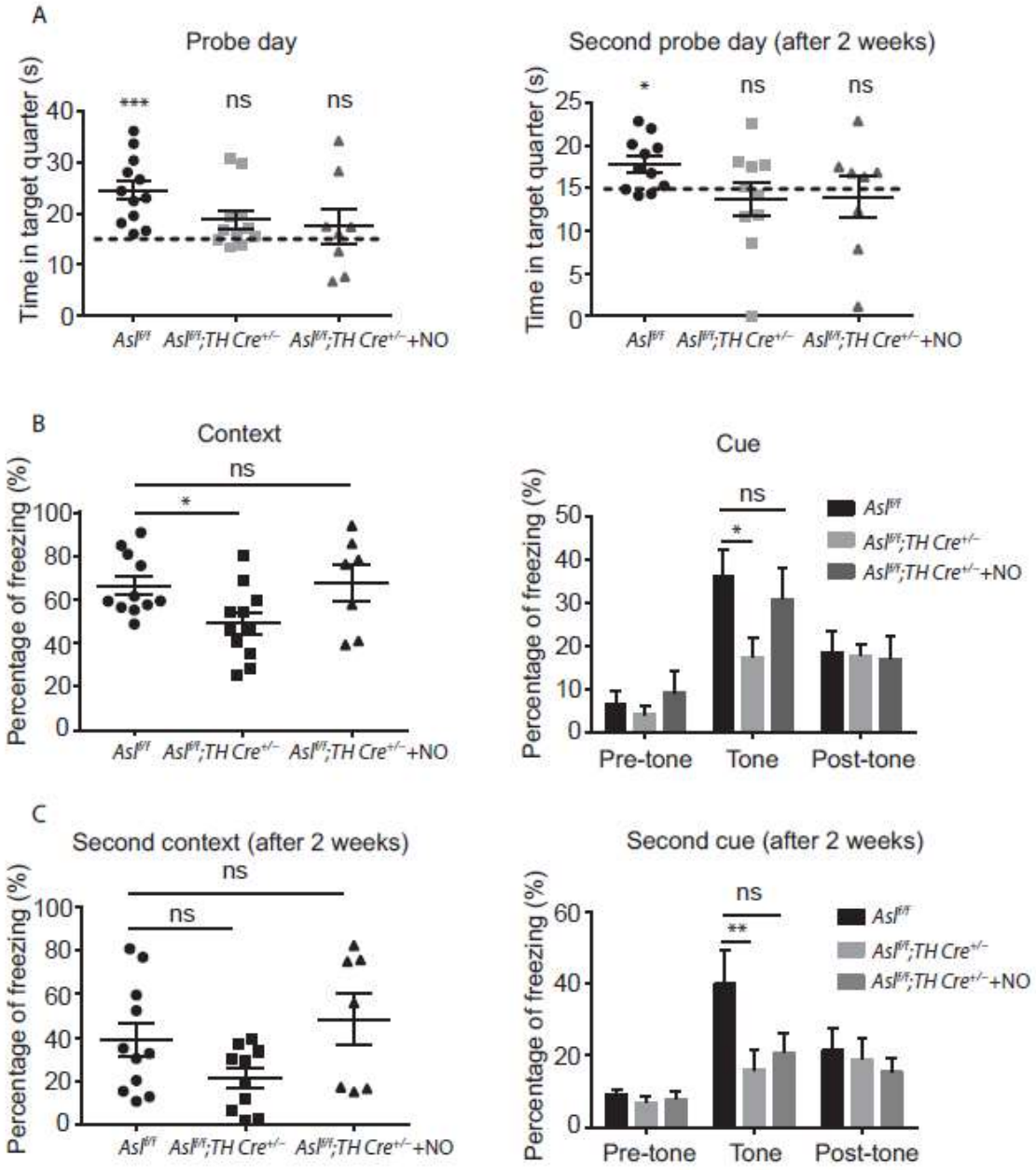

Figure 3: Adult *Asl$^{f/f}$;TH Cre$^{+/-}$* mice display cognitive deficits that can be partially rescued with NO donors.

(**A**) Adult *Asl$^{f/f}$* control group exhibit strong preference to the target quarter on probe day (left panel) and two weeks later (right panel), in comparison to adult *Asl$^{f/f}$;TH Cre$^{+/-}$* mice. Acute treatment with NO donor did not rescue the performance of *Asl$^{f/f}$;TH Cre$^{+/-}$* mice. The dotted line indicates the chance of time for each quarter. (**B**) Adult control mice trained for the fear conditioning paradigm and tested for demonstrating freezing responses to context (left panel) and cue (tone) challenges (right panel), froze significantly more than adult *Asl$^{f/f}$;TH Cre$^{+/-}$* mice. Acute treatment with NO donor rescue the performance of *Asl$^{f/f}$;TH Cre$^{+/-}$* mice. (**C**) Two weeks following the first fear-conditioning assessment, mice were tested again and showed the same trend in both the context (left panel) and cue (right panel) tests. ($n \geq 8$). Data represent mean ± s.e.m. (*p < 0.05, **p < 0.01, ***p<0.001, ****p<0.0001; ns- not significant).

Decreased TH levels following ASL loss promotes tyrosine aggregates and increased α- synuclein levels

Along with a decrease in catecholamine levels, a reduction in TH enzymatic activity would be expected to increase the levels of its substrate, tyrosine. Analysis of cerebrospinal fluid (CSF) from patients with ASLD who underwent liver transplantation, demonstrated higher than normal levels of tyrosine, while their plasma tyrosine levels remained within the normal ranges (**Figure 4A**). These results suggest that in spite of normalization of ASL function in the liver following the transplant, the tissue-autonomous loss from the central nervous system has biochemical, and potentially clinically relevant consequences. Although dopamine deficiency in the SNc and aggregation of proteins in neurons are the two main hallmarks of PD, a direct connection between these findings still remains indefinable (Mor, Daniels et al., 2019). High levels of tyrosine have been reported to lead to neurotoxic amyloid fibrils, and tyrosine assemblies can trigger a cytotoxic effect that decreases cell viability in SH-SY5Y neuronal cell line (Zaguri, Kreiser et al., 2018). Thus, we next evaluated the potential contribution of tyrosine accumulation to neuronal damage following ASL loss. Strikingly, knockdown of ASL in SH-SY5Y neuronal cells, caused a significant deposition of tyrosine aggregates and decreased viability in similar to the consequences of artificial insertion of tyrosine aggregates to neuronal cells (**Figure 4B-C**). Importantly, tyrosine aggregation could be reduced with NO supplementation (**Figure 4B**). Reduction in catecholamine levels and specifically of norepinephrine as we demonstrated to occur following ASL loss (Lerner et al., 2019), was shown to affect the expression of α-synuclein and to promote aggregate formation (Mittal, Bjornevik et al., 2017). Thus, we next measured α-synuclein protein levels and found elevated levels in *shASL* SH-SY5Y neuronal cells as compared to control cells (**Figure 4D**).

The identification of tyrosine aggregates together with high α-synuclein levels suggest that ASL loss may predispose potential seeding to aggregate formation in neurons. Following the rationale of our hypothesis for potential connection between ASLD and PD, we analyzed a recent GWAS dataset of PD (Nalls, Blauwendraat et al., 2019) and found that ASL is in close proximity to a risk variant for PD, alluding to potential association between genomic variants in ASL and PD (**Figure 4E**).

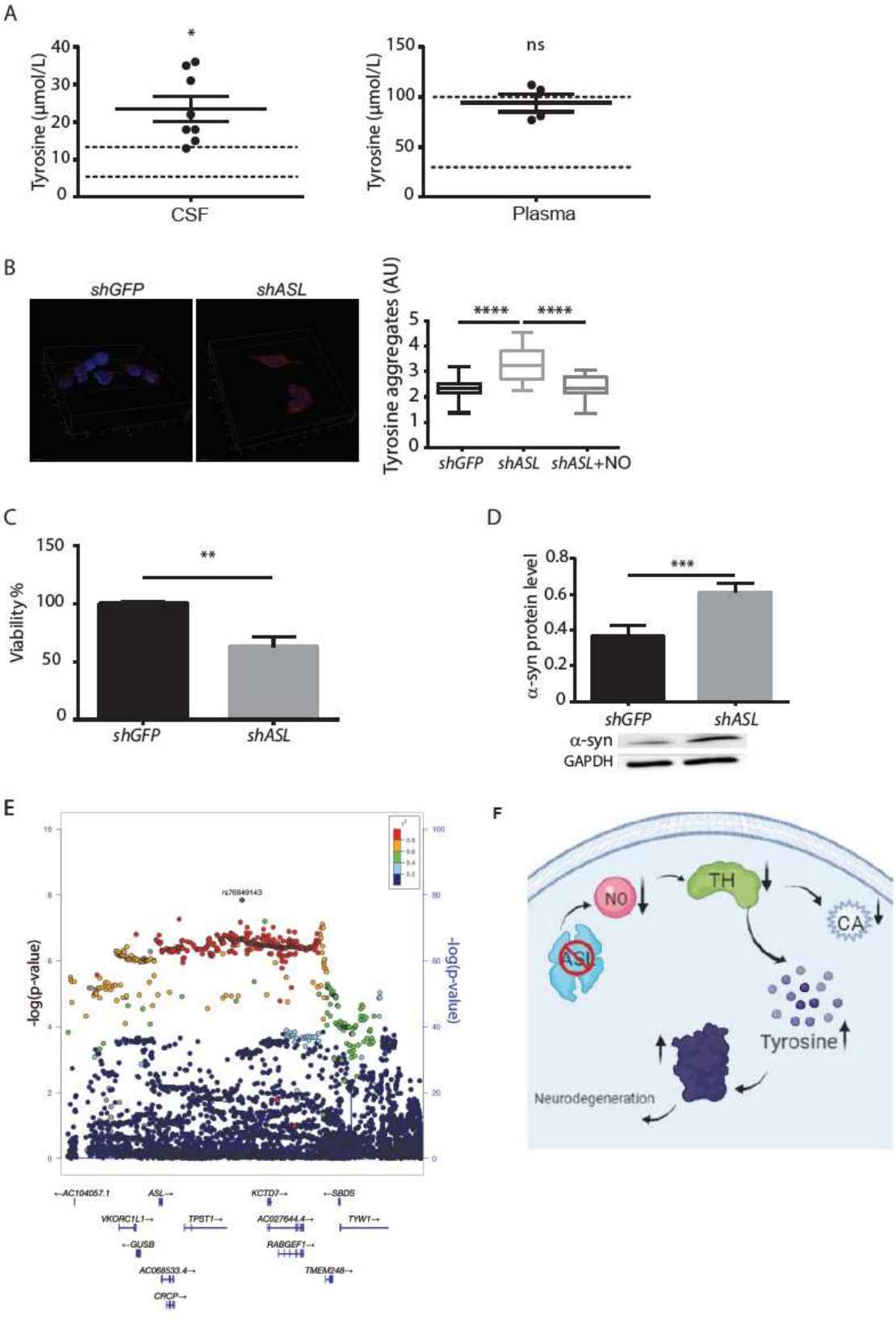

Figure 4: ASL deficiency in human patients associates with tyrosine accumulation and α-synuclein aggregation**.** (**A**) Tyrosine levels in the CSF (left panel) and plasma (right panel) of ASLD patients that

underwent liver transplantation. Dashed lines indicate the normal level range (n=8 for CSF, n=4 for plasma) ($p<0.02$ for CSF, $p=0.56$ for plasma). (**B**) SH-SY5Y neurons were stained with anti-tyrosine aggregates antibodies and visualized using confocal microscopy. Representative staining of DAPI (blue) and anti-tyrosine staining (red) are shown (Scale bars=10 μm). A representative 3D volume reconstruction of the Z-series with XZ-slice projection staining of control *shGFP* neurons (left panel) and *shASL* neurons (middle panel) (Interval between individual Z-stack serial images=0.5 μm). Right panel: quantification of the fluorescence intensity of the anti-tyrosine aggregates staining of *shGFP* and *shASL* neurons supplemented with or without NO donors ($n\geq14$) (One-way ANOVA with Bonferroni). (**C**) Measurements of neuronal cell viability following the addition of the XTT reagent. Absorbance was determined at 615 nm and 690 nm (n=4). (**D**) Quantification of α-synuclein protein levels from SH-SY5Y neuronal cells (n=4). Lower panel: representative western blot for α- synuclein levels. (**E**) ASL is located in close proximity to a PD locus variant identified by recent GWAS studies from the iPDGC Locus Browser v1.5 (32864809). The lead single nucleotide polymorphism (SNP) at this locus is rs76949143 (purple). Recombination rate peaks are marked in blue and variants are colored by their r2 linkage disequilibrium values. Data represent mean ± s.e.m. (*$p < 0.05$, **$p < 0.01$, ***$p<0.001$, ****$p<0.0001$; ns- not significant). (**F**) Summary model of our findings demonstrating that ASL loss leads to decreased TH activity, subsequently causing decreased catecholamine (CA) levels and accumulation of tyrosine which together with elevation of α- synuclein may predispose to aggregate formation.

Discussion

Individuals with ASLD suffer from neurocognitive deficits, seizures, and learning difficulties that can be out of proportion to the magnitude of hyperammonemia as compared to other UCDs (Baruteau, Jameson et al., 2017, Kolker, Garcia-Cazorla et al., 2015a, Kolker et al., 2015b, Waisbren, Gropman et al., 2016). Studies in murine models have shown that neuropathology associated with ASLD can be independent of hyperammonemia (Baruteau, Perocheau et al., 2018). ASL is the only enzyme in mammalians that is able to generate arginine, the substrate of NOS for the generation of NO. We and others have shown that ASLD is a human model of NO deficiency and that tissue-autonomous loss of ASL can be a model to study consequences of cell-specific NO deficiency (Jin, Kho et al., 2020) (Lerner et al., 2019) (Baruteau, Diez-Fernandez et al., 2019) (Kho et al., 2018) (Stettner et al., 2018) (Premkumar, Sule et al., 2014) (Nagamani et al., 2012) (Baruteau et al., 2019). Additionally, we have recently shown that ASL is expressed prominently in the noradrenergic nucleus-the locus coeruleus (LC), and that ASL participates in the regulation of catecholamine synthesis by NO *via* nitrosylation of TH (Lerner et al., 2019, Wang, Sung et al., 2017). Thus ASLD is a useful model to study a disease processes that involves dysregulation of NO and catecholamines like PD.

Data from humans as well as from experimental models of PD support a role for NO in modulating the inflammation, oxidative stress, mitochondrial dysfunction, and excitotoxicity-mediated

neuronal injury in PD (Jimenez-Jimenez, Alonso-Navarro et al., 2016). These data demonstrate that NO can play both neuroprotective as well as neurotoxic roles in dependence with NO cell of origin e.g, an immune cell or neuron. In addition, neuronal damage has been shown to be caused by both high NO levels as well as by high levels of NO related free radicals as nitrotyrosine, a product of tyrosine nitration mediated by pyroxynitrite (Good, Hsu et al., 1998). Interestingly, depletion of arginine following ASL loss, promotes the uncoupling of NOS and subsequently, to the formation of NO related free radicals (Xia, Dawson et al., 1996), (Erez, Nagamani et al., 2011b). Together, these data led us to dissect a potential role for ASL metabolism in PD in a cell specific manner.

Here, we show that ASL is specifically expressed in a unique subpopulation of dopaminergic neurons, the SNc – ALDH1A1^{+} cells, which are known to have a significant vulnerability to the neuronal damage observed in PD, and are consequently involved in the causation of the movement-related disease manifestations. We also demonstrate that mice with loss of ASL in these dopaminergic neurons phenocopy the memory and motor deficits that are observed in murine models of PD. Interestingly, the levels of ALDHA1, one of the biomarkers suggestive of a diagnosis of PD in humans (Grunblatt et al., 2010), were elevated in the CSF of *Asl$^{f/f}$;TH Cre$^{+/-}$* mice. Our data thus allude to the potential link between ASL, TH, and catecholamine depletion, to the pathogenesis of certain forms of neurodegenerative disorders involving the nigrostriatal system, such as PD.

The pathological hallmark of PD is accumulation of protein aggregates and specifically of α-synuclein in the neurons of the SNc. Mechanistically, these aggregations are thought to damage neurons in the SNc and cause abnormalities in catecholamine levels, mainly of dopamine. To date, the cause of the accumulation and aggregation of proteins specifically in these neurons of PD patients is unknown. One potential explanation comes from the “seeding” theory, which suggests that accumulation of amino acids may form a seed for the formation of larger aggregates of α-synuclein (Anand, Dubey et al., 2017, Shaham-Niv, Adler-Abramovich et al., 2015, Tavassoly et al., 2018).

Inborn metabolic diseases have an innate risk for accumulation of different metabolites (Sade, Shaham-Niv et al., 2018). Tyrosine aggregations have been described in the cornea and skin of patients with tyrosinemia type II, a congenital metabolic disease caused by deficiency of the enzyme tyrosine aminotransferase (1968) . Here, we describe that reduction of ASL in neurons leads to reduction in TH activity and to accumulation of tyrosine. This reduction in TH activity results in a dual damage- a reduction in catecholamine levels and in accumulation of tyrosine specifically in neurons. We further demonstrate an accumulation of tyrosine in CSF of ASLD patients even after

liver transplantation. Interestingly, patients with PD have also been shown to have high levels of tyrosine in their CSF (D'Andrea, Pizzolato et al., 2019, Jimenez-Jimenez, Alonso-Navarro et al., 2020), and nitrotyrosine immunoreactivity has been found in the core of Lewy bodies within degenerating neurons in PD patients' brain (Jimenez-Jimenez et al., 2016), supporting the relevance of tyrosine accumulation to PD. Collectively, our data may suggest that neurons of the SNc depend on TH for dopamine synthesis and are hence particularly sensitive to tyrosine accumulation. Our findings that neuronal loss of ASL leads to elevation of α-synuclein levels, further support a model in which deficiency in ASL specifically in catecholamine synthesis neurons cause reduction in TH levels that result in accumulation of tyrosine that can potentially leads to aggregation in TH neurons (**Figure 4F**).

Rare disorders as inborn error of metabolism, offer us a unique prism to understand the contribution of mutations in single enzymes to the pathogenesis of complex diseases (Erez & DeBerardinis, 2015). Here, we illustrate this point by dissecting the role ASL plays in the SNc, and by shedding light on potential metabolic association between ASL and SNc-related neurodegenerative disorders such as PD. Importantly, our work suggests translational implications for further exploring potential use of NO supplementation in dopaminergic related pathologies.

Acknowledgments

We acknowledge and thank the Weizmann Institute for providing financial and infrastructural support. AE is supported by research grants from the European research program (ERC818943), and from the Israel Science Foundation (860/18). AE received additional support from The Moross Integrated Cancer Center, Sagol Institute for Longevity Research, Adelis Foundation, Rising Tide Foundation, and from Manya and Adolph Zarovinsky.

Members of the UCDC include Nicholas Ah Mew, Matthias R. Baumgartner, Jirair K. Bedoyan, Gerard Berry, Susan A. Berry, Peter Burgard, Lindsay Burrage, Curtis Coughlin, George A. Diaz, Gregory Enns, Renata C. Gallagher, Andrea Gropman, Cary O. Harding, Georg Hoffmann, Cynthia Le Mons, Shawn E. McCandless, J. Lawrence Merritt II, Sandesh CS Nagamani, Andreas Schulze, Jennifer Seminara, Tamar Stricker, Mendel Tuchman, Susan Waisbren, James D. Weisfeld-Adams, Derek Wong, and Marc Yudkoff.

The UCDC (U54HD061221) is a part of the National Institutes of Health (NIH) Rare Disease Clinical Research Network (RDCRN), supported through collaboration between the Office of Rare Diseases Research (ORDR), the National Center for Advancing Translational Science (NCATS), the Eunice Kennedy Shriver National Institute of Child Health and Human Development (NICHD), and

the National Institute of Diabetes and Digestive and Kidney Diseases (NIDDK). The UCDC is also supported by the O'Malley Foundation, the Kettering Fund, and the National Urea Cycle Disorders Foundation. The contents of this manuscript are solely the responsibility of the authors and they do not necessarily represent the official views of the NICHD or the National Institutes of Health. Figure 4F was generated using BioRender.com.

Authors declare no conflict of interest.

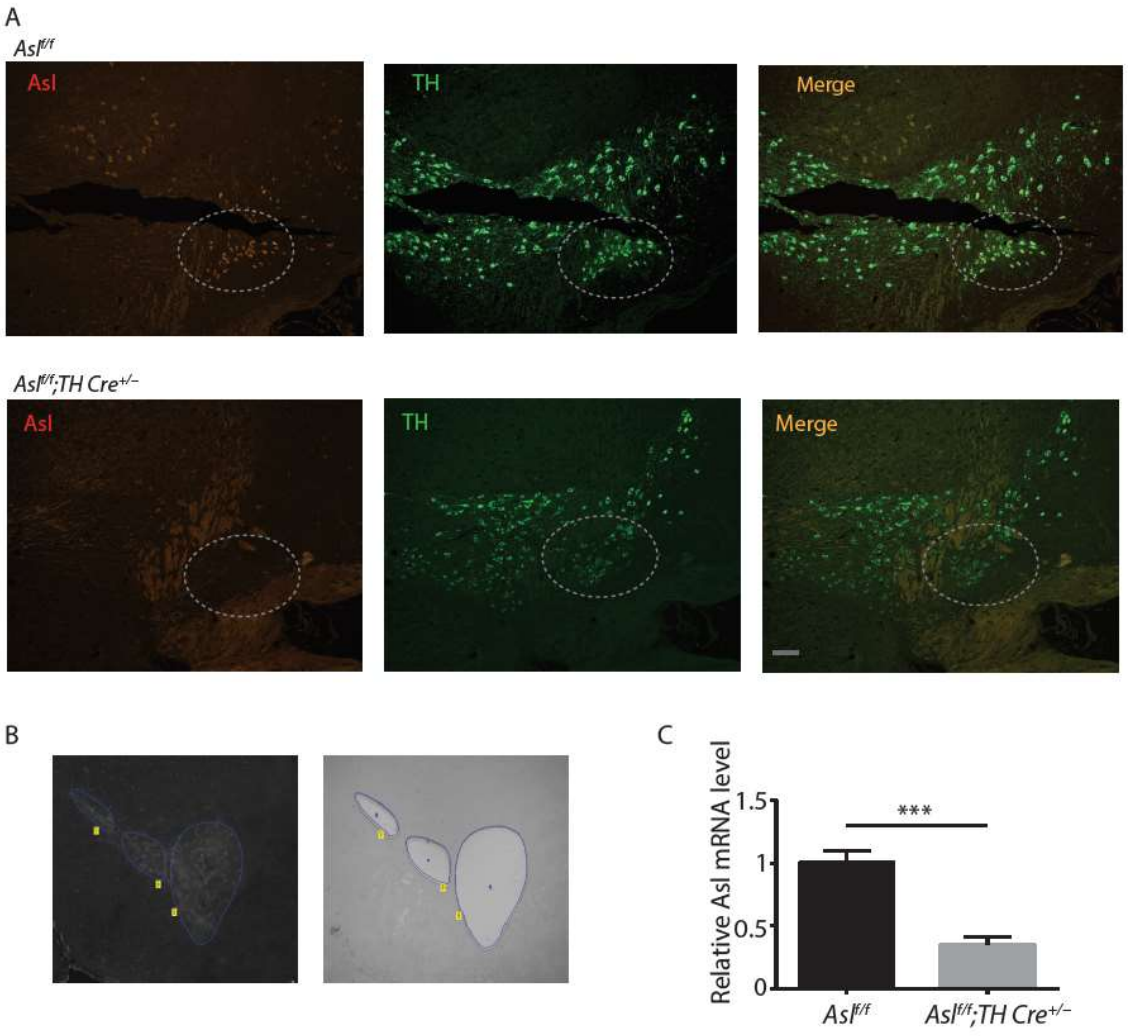

Supplementary figure legends: ASL KO in ALDH1A1^{+}neurons in the SNc.

(**A**) ASL expression in the SNc of wild-type mice (top left) and co-localized with TH (top right). ASL as well as TH are deficient specifically in the SNcM (indicated by dashed line) of *Asl$^{f/f}$;TH Cre$^{+/-}$* mice (lower panel). (Scale bar=250 µm). (**B**) A representative fresh-frozen brain section of the SNc and VTA stained with TH antibody before (left panel) and after laser micro-dissection (right panel). (**C**) Quantification of *Asl* mRNA isolated by laser microdissection from the LC of *Asl$^{f/f}$;TH Cre$^{+/-}$* and from *Asl$^{f/f}$* control mice as measured by RT-PCR with specific TaqMan probes (n=7 mice in each group).

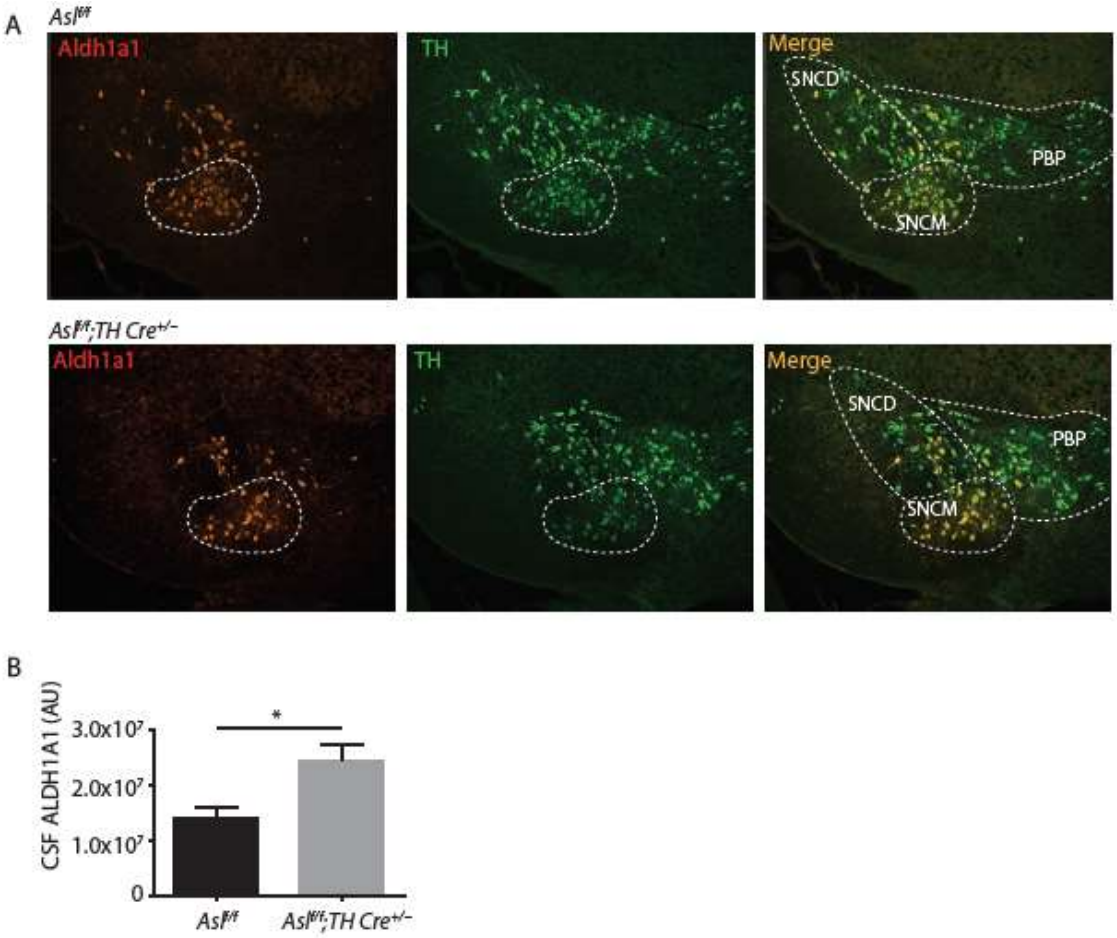

Supplementary figure 2: ASL KO in catecholamine neurons results in abnormal TH levels in the SNc and abnormal ALDH1A1 levels in the CSF.

(**A**) Representative images of TH expression in ALDH1A1^{+} neurons in the SNcM. Dashed lines differentiates the SNc and VTA subregions. (**B**) ALDH1A1protein levels in the CSF of adult *Asl$^{f/f}$;TH Cre$^{+/-}$* and *Asl$^{f/f}$* control mice (n=5 mice in each group). SNcM-SNc medial, SNcD-SNc dorsal, PBP-parabrachial pigmented nucleus.

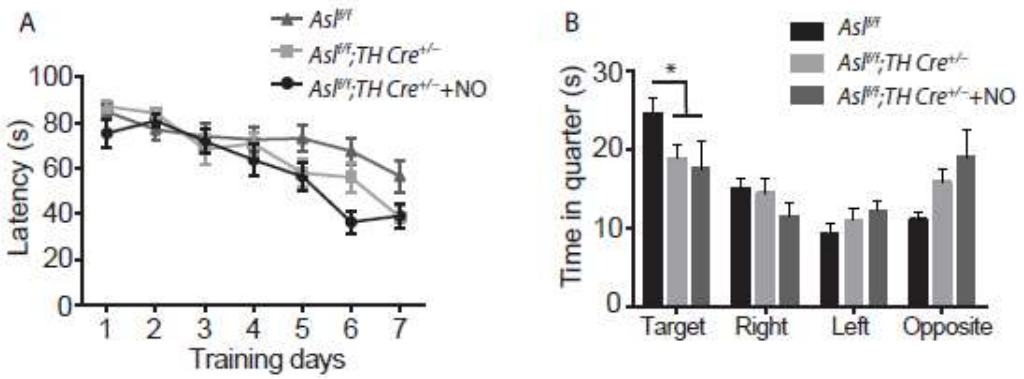

Supplementary figure 3: Adult *Asl$^{f/f}$;TH Cre$^{+/-}$* mice demonstrate long memory impairments in Morris Water Maze test.

(**A**) Spatial memory was evaluated two days following the last training session. Adult *Asl$^{f/f}$* control group spent significantly longer times in the target quarter as compared to adult *Asl$^{f/f}$;TH Cre$^{+/-}$* mice. (**B**) For 7 consecutive learning days adult mice did not show any significant differences in the length of time spent on finding the platform (n≥ 8). Data represent mean ± s.e.m. (*p < 0.05).

Methods

Human studies

The Urea Cycle Disorders Consortium (UCDC) of the National Institutes of Health Rare Diseases Clinical Research Network (RDCRN) currently consists of 16 clinical sites across the United States, Canada, and Europe. Clinical data presented in this report were collected in a standardized format according to a manual of operations as part of the Longitudinal Study of Urea Cycle Disorders (NCT00237315), an ongoing natural history study being conducted by the consortium since 2006. This study was approved by the Institutional Review Boards (IRB) of all clinical sites of the UCDC between 2006 and 2015. Since 2015, the IRB at Children's National Medical Center has been serving as the central IRB for the consortium. Informed consent was obtained from all participants or their parents or legal guardians. For the Longitudinal Study of Urea Cycle Disorders, clinical, laboratory, and neuropsychological data are collected. For the analyses presented here, the following data were collected from individuals with ASLD and ASS1D: gender, age, presence or absence of at least one hyperammonemic episode (defined as plasma ammonia levels greater than 100 µmol/L), presence or absence of tremors.

Human CSF samples

CSF and plasma samples were obtained as part of the standard liver transplant protocol at the Bambino Gesù Childrens Hospital in Rome. The studies were performed in accordance with the Declaration of Helsinki and approved by the Ethical Committee (2119_OPBG_2020). The age of the patients range between 2.5-12.0 years.

GWAS analysis

Method: Parkinson's Disease GWAS Locus Browser. The iPDGC Locus Browser v1.3.1 (https://pdgenetics.shinyapps.io/GWASBrowser/) combines data from multiple databases and recent large-scale genome-wide association studies (GWAS) for Parkinson's disease (PD)(Grenn, Kim et al., 2020). 92 genome-wide significant PD GWAS variant loci are presented with the genes most associated with the variant of interest 1 Megabase (Mb) up and downstream based on self-ranked criteria and based on the hg19 reference genome (Haeussler, Zweig et al., 2019).

Animal studies

All animal procedures were approved by the Institutional Animal Care and Use Committee (applications number: 07201118-1) and were performed in strict adherence to Weizmann Institute Animal Care and Use guidelines. C57BL/6JOlaHsd mice were purchased from ENVIGO RMS (ISRAEL). The B6.Cg-Tg(Th-cre)1Tmd/J were kindly given to us by Dr. Ofer Yizhar (Madisen, Zwingman et al., 2010). Mice were monitored daily by Weizmann Institute staff and veterinary personnel for health and activity. Mice were given *ad libitum* access to water and standard mouse chow with 12-hr light/dark cycles. Littermates of age and gender matched mice were randomly assigned to experimental groups.

Cell cultures

SH-SY5Y human neuroblastoma cells (American Type Culture Collection, ATCC, Manassas, VA, USA) were grown in DMEM (Dulbecco's modified Eagle's medium) supplemented with 10% heat-inactivated FBS, 100 units/mL streptomycin, and 100 µg/mL penicillin at 37°C in a humidified 5% CO_2 atmosphere. All cells were tested routinely for mycoplasma using a Mycoplasma EZ-PCR test kit (20–700-20, Biological Industries).

Virus infection

HEK293T cells were used to package the lentivirus. HEK293T cells in the logarithmic growth phase were seeded into a 10 cm plate. Once cell confluence reached 80%, viral packaging mix (Renium K4975-00) and 1 µg of either *shGFP* or *shASL* were co-transfected into HEK293T cells with the aid of lipofectamine 2000. 48 h after transfection, the supernatant of HEK293T cells was collected and centrifuged (1000 rpm) at 4 °C for 10 min to remove cell debris. SH-SY5Y cells were seeded in 6-well plates (200,000 cells/well) and grown to reach approximately 80% confluency. 0.5 ml of the supernatant was added to the cell culture medium without Penicillin-Streptomycin and incubated with the cells for 12 h. In the next day, the medium was replaced by fresh medium. The cells were then transferred to a 10 cm plate and Puromycin (4 µg/mL) was added for 4 days.

Cell viability experiments

Cells were incubated in medium without serum for 24 h (100 µl). After incubation cell viability was evaluated using the XTT cell proliferation assay kit (Biological Industries) according to the manufacturer's instructions. Briefly, 100 µl of the activation reagent was added to 5 ml of the XTT reagent, followed by the addition of 50 µl of activated XTT solution to each well. After 3 h of incubation at 37 °C, color intensity was measured using an enzyme-linked immunosorbent assay (ELISA) microplate reader at 450 and 630 nm.

Mice perfusion

Following euthanasia, mice were rapidly perfused with cold 4% paraformaldehyde (PFA) in PBS. Mice brains were rapidly removed, immersed in freshly 4% PFA for 24 h, and then transmitted to 1% PFA for 24 h. For *in-situ* hybridization mouse brains were placed in 1× PBS with 30% sucrose for another

24 h and then frozen and sectioned in coronal plane using a microtome. For immunostaining mouse brains were embedded in paraffin.

NO treatment

For *in vitro* assays, 100 µM S-Nitroso-N-acetyl-DL-penicillamine (SNAP) (CayMan chemicals 82250) was added to the medium 24 h before cell collection. For *in vivo* rescue experiments, mice were treated with $NaNO_2$ 100 mg/kg/d in drinking water, renewed every 3 days (Sigma-Aldrich, St. Louis, MO, catalog number S2252).

Catecholamine analysis

Extraction

The extraction procedure was performed at 4 °C. Pre-weighted samples in 1.5-mL test tubes were spin shortly (21,000 g, 15 sec) to place them at the bottom. 50 µL of 4% perchloric acid containing IS mix (NorLeu 2 µM; Arg-13C6 12 µM; NEN-D6 20 ng/ml; DA-D4 40 ng/ml; ST-D4 400 ng/ml) was added, and the mixture was homogenized using handheld grinder (Agros), followed by agitation in shaker (1200 rpm, 30 min, ThermoMixer C, Eppendorf) and centrifuged (20,000 g, 10 min). The collected supernatants were used for further analysis.

Derivatization

Derivatization procedure was performed using AQC reagent synthesized as described (Cohen & Michaud, 1993). Briefly, a 10-µL aliquot of the sample or standard solution (with the internal standards added) and 70 µL of 0.15 M sodium borate solution, pH 8.8 were derivatized with 20 µL of AQC in acetonitrile (2.7 mg/mL) by heating at 55 °C for 10 min. The reaction mixtures were cooled and placed in nanofilter vials (Thomson, 0.2 µm PES) for LC-MS.

LC-MS/MS analysis

The LC-MS/MS instrument consisted of Acquity I-class UPLC system (Waters) and Xevo TQ-S triple quadrupole mass spectrometer (Waters) equipped with an electrospray ion source and operated in positive ion mode was used for analysis. MassLynx and TargetLynx software (v.4.1, Waters) were applied for the acquisition and analysis of data. Chromatographic separation was done on a 150 x 2.1-mm i.d. 1.8-µm UPLC HSS T3 column equipped with 50 x 2.1-mm i.d., 1.8-µm UPLC HSS T3 pre-column (both Waters Acquity) with 0.1% formic acid as mobile phase A and 0.1% formic acid in acetonitrile as B at a flow rate of 0.6 ml/min and column temperature 45 °C. A gradient was as follows: 0.5 min the column was hold at 4%B, then linear increase to 10%B in 2 min, then to 28%B in 2.5 min, and to 95%B in 0.1 min. Just after back to 0%B during 1.1 min, and equilibration at 4%B for 1.3 minutes. Samples kept at ambient temperature (23 °C) were automatically injected in a volume of 1 µl. For mass spectrometry argon was used as the collision gas with flow 0.10 ml/min. The capillary voltage was set to 3.00 kV, cone voltage 25V, source offset 30V, source temperature 150 °C, desolvation temperature 650 °C, desolvation gas flow 800 L/hr, cone gas flow 150 L/hr. Analytes were detected using corresponding selected reaction monitoring (SRM) and retention times as shown in the table. The concentrations based on standard curves were calculated using TargetLynx (Waters).

Laser micro-dissection (LMD)

Brains were removed rapidly, briefly washed in cold PBS, embedded and frozen in OCT on dry ice without fixation. 8 µm thick sections were cut from the frozen block, mounted on polyethylene membrane-coated glass slides (Zeiss, A4151909081000), air-dried for 1 min at room temperature and put in -80 °C. At the day of the experiment, slides were thawed for 5 min in room temperature followed by fixation in 70% ethanol (30 s), incubation in DEPC water (1 min), stained with TH antibody (ab209921, 10 min), washed vigorously with PBS (30 s) and air dried for 3 min before microdissection.

The cutting was performed with the following parameters: PALM 20X lens, cut energy 45 (1-100), cut focus 65 (1-100). Tissue fragments were catapulted and collected in 0.2 ml adhesive cap tubes (Zeiss, A4151909181000) with these settings: LPC energy 50 (1-100), LPC focus 63 (1-100). The capturing success was visually confirmed by focusing the PALM on the targeted adhesive cap after the collection session.

Behavioral studies

CatWalk

This system was used for quantitative assessment of footfalls and gait. The apparatus consists of an enclosed walkway that a mouse walks on; the "Illuminated Footprints" technology allows a high-speed video camera (positioned underneath the walkway) to capture the footprints (Noldus, Wageningen, Netherlands). These images are processed based on the dimensions, position and dynamics of each footfall to produce quantitative analyses of footfalls and gait: each mouse went through a test session that was comprised of five "runs" (the mouse walks the full length of a 50 cm runway) that comply with minimal speed variation requirements (less than 40%).

Morris water maze

We studied possible alterations of spatial memory in the Morris water maze. The water maze consisted of a circular tank (120 cm diameter) with a removable escape platform centered in one of the four maze quadrants. In the testing room, only distal visual-spatial cues for locating the hidden platform were available. During testing, the tank is filled with 24 ˚C water clouded with milk powder. Acquisition phase. The mice were subjected to 4 trials per day with an inter-trial interval of 10 min, for 7 consecutive days. In each trial, the mice were required to find a platform located in one of the four quadrant submerged 1 cm below the water surface. The escape latency in each trial was recorded up to 90 s. Each mouse was allowed to remain on the platform for 15 s and was then removed from the maze. If the mouse did not escape in the allocated time, it was manually placed on the platform for 15 s. Memory was assessed 24 h after the last trial. The escape platform was removed and mice were allowed to search for it for 1 min, and the time spent swimming in the different quadrants of the pool was monitored using an automated tracking system (Noldus, Wageningen, Netherlands).

Fear conditioning

The fear-conditioning paradigm was used to study possible alteration of hippocampal or amygdala-dependent forms of memories. A computer-controlled fear-conditioning system (Noldus, Wageningen, Netherlands) monitors the procedure while measuring freezing behavior (i.e., lack of movement except respiration). The test is performed within three days as previously described (Neufeld-Cohen, Tsoory et al., 2010): 1) Habituation: on the first day, mice are habituated for 5 min to the fear conditioning chamber, a clear Plexiglas cage (21 cm x 20 cm x 36 cm) with a stainless steel floor grid within a constantly illuminated (250 lx) fear-conditioning housing. 2) Conditioning: conditioning takes place on day 2 in one 5-min training session. Mice initially explore the context for 2 min. Thereafter, two pairings of a co-terminating tone [conditioned stimulus (CS): 30 s, 3,000 Hz, pulsed 10 Hz, 80 dB (A)] and shock [unconditioned stimulus (US): 0.7 mA, 2 s, constant current) with a fixed ITI of 60 s. The US is delivered through the metal grid floor. Mice are removed from this chamber 1 min after the last CS–US pairing. The chamber is cleaned with 10% ethanol before each session. The ventilating fan of the conditioning box housing provides a constant auditory background noise [white noise, 62 dB(A)]. 3) Testing: Context dependent memory is tested 24 h after the conditioning by re-exposure to the conditioning box for 5 min without any stimuli. The Cue dependent memory is tested 1 h after the Context test by exposure to the conditioned [conditioned stimulus (CS): 30 s, 3,000 Hz, pulsed 10 Hz, 80 dB (A)] in different environmental conditions (black

Plexiglas box, black floor instead of metal grid, no illumination, no ventilation noise, cleaning solution: acetic acid 10% instead of alcohol 10%).

Brain tissue biopsies collection

Immediately after decapitation, mouse brains were removed and placed in 1.0 mm coronal slice intervals brain matrix (BSMAS001-1 Civic Instruments). The brains were sliced using standard razor blades into 2-mm slices that were frozen immediately on dry ice. The areas of interest were punched using a microdissecting 16G needle according to the anatomical references of The Mouse Brain in Stereotaxic Coordinates (axinos F, Franklin KBJ (2001). The brains were stored immediately at−80 °C for later use.

Immunostaining

In-vivo: Four-micrometer paraffin embedded tissue sections were deparaffinized by xylene and rehydrated through a gradient of ethanol. Sections were exposed to acetone for 7 min at −20 °C and antigens were retrieved in citric acid in a microwave oven at full-intensity for 3 min until boiling point was reached, and then at 20% intensity for 10 min. Blocking of nonspecific binding was done with 20% normal horse serum and 0.2-0.5% triton for 90 min in a humidity chamber. Sections were incubated with the primary antibodies as follow; ASL (1:100, Abcam, ab97370); TH (1:500, millipore AB1542). All antibodies were diluted in PBS containing 2% normal horse serum and 0.2% Triton. Sections were incubated overnight at RT followed by 48 h at 4 °C. Sections were washed three times in PBS and incubated with biotinylated anti-rabbit antibody for 90 min in a humidity chamber, washed, and incubated with streptavidin Cy2 and Cy3 anti-goat antibodies (all from Jackson ImmunoResearch) for 40 min. Sections were counterstained by Hoechst (Molecular Probes). Stained sections were examined and photographed with a fluorescence microscope (Eclipse Ni-U; Nikon) equipped with Plan Fluor objectives (20x;40x) connected to a color camera (DS-Ri1, Nikon) microscope.

Excitation/emission wavelengths were 412/450 nm for DAPI and 548/561 nm for Cy3.

In-vitro: cells were grown to 70% confluence on poly-L-lysine coated cover-slips in 24-well plates. The cells were then rinsed with PBS and fixed in 4% PFA for 15 min at room temperature. The cells were washed twice with ice-cold PBS and treated with 0.25% Triton X-100 for 10 min at room temperature to allow cellular permeabilization. After thoroughly washing the cells, blocking was performed using 1% BSA for 30 min at room temperature. Then, the cells were stained using a rabbit polyclonal anti-tyrosine antibody diluted 1:200 in blocking solution, for overnight incubation at 4 ◦C. The slides were washed three times with PBS and anti-rabbit Cy3-conjugated secondary antibody diluted 1:200 in blocking solution was added for 30 min at room temperature in the dark. Finally, cells were washed three times and the cover slips were mounted using 15 µL Vectashield Antifade Mounting Medium with DAPI. Imaging was performed using SP8 inverted confocal microscopy. Excitation/emission wavelengths were 412/450 nm for DAPI and 548/561 nm for Cy3. The fluorescence intensity was quantified using imageJ software.

Western blotting

Cells were lysed in RIPA and 1:100 protease inhibitor (Sigma-Aldrich). After centrifugation, the supernatant was collected, and protein content was evaluated by the BCA protein assay kit (Thermo Fisher 23225). 80 µg of each sample under reducing conditions were loaded into each lane and separated by electrophoresis on a 10% SDS polyacrylamide gel. Following electrophoresis, proteins were transferred to Immobilon transfer membranes (Tamar). Non-specific binding was blocked by incubation with 5% milk in TBST (10 mM Tris–HCl (pH 8.0), 150 mM NaCl, 0.1% Tween 20) for 1 h at 25 °C. Membranes were subsequently incubated with antibodies against ASL (1:500, ab97370,

Abcam), p97 (1:10,000, PA5-22257, Thermo Scientific), GAPDH (1:1,0000, ab128915, Abcam), TH (1:500, CST-2792S, cell signaling) $\alpha-$ synuclein. Antibody was detected using peroxidase-conjugated AffiniPure goat anti-rabbit IgG or goat anti-mouse IgG (Jackson ImmunoResearch) and enhanced using chemiluminescence western blotting detection reagents (Pierce™ ECL Western Blotting Substrate, Thermo Fisher). Gels were quantified by Gel Doc XR+ (BioRad) and analyzed by ImageLab 6.0 software (BioRad). The band area was calculated by the intensity of the band divided by the value obtained from the loading control.

RNA extraction and complementary DNA (cDNA) synthesis

RNA was extracted from cells using RNeasy Mini Kit (74104, QIAGEN). cDNA was synthesized from 1 µg RNA by using qScript cDNA Synthesis Kit (Quanta). Quantitative PCR was performed using SYBR green PCR master mix (Thermo Fisher scientific 4385612) or with TaqMan Real-Time PCR Master Mix (Thermo Fisher scientific 4444557).

Proteomic analysis for CSF collection

Sample preparation

All chemicals were ordered from Sigma unless otherwise noted. 10-20 µl of CSF were mixed with 8 M urea. Proteins were reduced with 5 mM dithiothreitol for 1 h at room temperature, and alkylated with 10 mM iodoacetamide in the dark for 45 min at room temperature. Samples were diluted to 2 M urea with 50 mM ammonium bicarbonate. Proteins were then subjected to digestion with trypsin (Promega; Madison, WI, USA) overnight at 37 °C at 50:1 protein:trypsin ratio, followed by a second trypsin digestion for 4 h. The digestions were stopped by addition of trifluroacetic acid (1% final concentration). Following digestion, peptides were desalted using Oasis HLB, µElution format (Waters, Milford, MA, USA). The samples were vacuum dried and stored in -80 ˚C until further analysis.

Liquid chromatography

ULC/MS grade solvents were used for all chromatographic steps. Each sample was loaded using split-less nano-Ultra Performance Liquid Chromatography (10 kpsi nanoAcquity; Waters, Milford, MA, USA). The mobile phase was: A) H_2O + 0.1% formic acid and B) acetonitrile + 0.1% formic acid. Desalting of the samples was performed online using a reversed-phase Symmetry C18 trapping column (180 µm internal diameter, 20 mm length, 5 µm particle size; Waters). The peptides were then separated using a T3 HSS nano-column (75 µm internal diameter, 250 mm length, 1.8 µm particle size; Waters) at 0.35 µL/min. Peptides were eluted from the column into the mass spectrometer using the following gradient: 4% to 27%B in 105 min, 27% to 90%B in 5 min, maintained at 90% for 5 min and then back to initial conditions.

Mass Spectrometry

The nanoUPLC was coupled online through a nanoESI emitter (10 µm tip; New Objective; Woburn, MA, USA) to a quadrupole orbitrap mass spectrometer (HFX , Thermo Scientific) using a FlexIon nanospray apparatus (Proxeon). Data was acquired in data dependent acquisition (DDA) mode, using a Top10 method. MS1 resolution was set to 120,000 (at 400 m/z), mass range of 375-1650 m/z, AGC of 1e6 and maximum injection time was set to 60 msec. MS2 resolution was set to 15,000, quadrupole isolation 1.7 m/z, AGC of 1e5, dynamic exclusion of 30 sec and maximum injection time of 60 msec. A preferential inclusion list was specified for higher priority of MS/MS triggering. The list of peptides is provided as Supplementary file.

Data processing

Raw data was processed with MaxQuant v1.6.6.0 using the default parameters except the following: LFQ min. ratio count = 1, separate LFQ in parameter groups (young mice vs. old mice) and match between runs were enabled. The data was searched with the Andromeda search engine against the murine proteome database (November 2019 version) appended with common lab protein contaminants and the following modifications: Carbamidomethylation of C as a fixed modification and oxidation of M and protein N-terminal acetylation as variable ones. The LFQ (Label-Free Quantification) intensities were calculated and used for further calculations using Perseus v1.6.2.3. Decoy hits were filtered out, as well as proteins that were identified on the basis of a modified peptide only. The LFQ intensities were log2 transformed and only proteins that had at least 4 valid values in at least one experimental group were kept. The remaining missing values were imputed. Statistical analysis was done using a Student's t-test.

Statistical Analysis

Unless indicate otherwise, values are expressed as mean ± SEM. Statistical analysis was performed using repeated-measures two-way ANOVA with Bonferroni post hoc t tests or Student's t tests as appropriate. Statistical details of individual experiments such as exact values of n can be found in figures and legends. The sample size was chosen in advance based on common practice of the described experiment, and is mentioned for each experiment. Each experiment was conducted with biological and technical replicates and repeated at least three times. Statistical tests were done using Prism software (GraphPad Software). $P<0.05$ was considered significant in all analyses (* denotes $P<0.05$, **$P<0.005$, ***$P<0.0005$, **** $P<0.0001$).

References

(1968) Disorders of tyrosine metabolism. *Br Med J* 3: 511-2

Anand BG, Dubey K, Shekhawat DS, Kar K (2017) Intrinsic property of phenylalanine to trigger protein aggregation and hemolysis has a direct relevance to phenylketonuria. *Sci Rep* 7: 11146

Baruteau J, Diez-Fernandez C, Lerner S, Ranucci G, Gissen P, Dionisi-Vici C, Nagamani S, Erez A, Haberle J (2019) Argininosuccinic aciduria: Recent pathophysiological insights and therapeutic prospects. *J Inherit Metab Dis* 42: 1147-1161

Baruteau J, Jameson E, Morris AA, Chakrapani A, Santra S, Vijay S, Kocadag H, Beesley CE, Grunewald S, Murphy E, Cleary M, Mundy H, Abulhoul L, Broomfield A, Lachmann R, Rahman Y, Robinson PH, MacPherson L, Foster K, Chong WK et al. (2017) Expanding the phenotype in argininosuccinic aciduria: need for new therapies. *J Inherit Metab Dis* 40: 357-368

Baruteau J, Perocheau DP, Hanley J, Lorvellec M, Rocha-Ferreira E, Karda R, Ng J, Suff N, Diaz JA, Rahim AA, Hughes MP, Banushi B, Prunty H, Hristova M, Ridout DA, Virasami A, Heales S, Howe SJ, Buckley SMK, Mills PB et al. (2018) Argininosuccinic aciduria fosters neuronal nitrosative stress reversed by Asl gene transfer. *Nat Commun* 9: 3505

Boix J, von Hieber D, Connor B (2018) Gait Analysis for Early Detection of Motor Symptoms in the 6-OHDA Rat Model of Parkinson's Disease. *Front Behav Neurosci* 12: 39

Buxbaum JN, Linke RP (2012) A molecular history of the amyloidoses. *J Mol Biol* 421: 142-59

Cai H, Liu G, Sun L, Ding J (2014) Aldehyde Dehydrogenase 1 making molecular inroads into the differential vulnerability of nigrostriatal dopaminergic neuron subtypes in Parkinson's disease. *Transl Neurodegener* 3: 27

Chrousos GP (2009) Stress and disorders of the stress system. *Nat Rev Endocrinol* 5: 374-81

Cohen SA, Michaud DP (1993) Synthesis of a fluorescent derivatizing reagent, 6-aminoquinolyl-N-hydroxysuccinimidyl carbamate, and its application for the analysis of hydrolysate amino acids via high-performance liquid chromatography. *Anal Biochem* 211: 279-87

D'Andrea G, Pizzolato G, Gucciardi A, Stocchero M, Giordano G, Baraldi E, Leon A (2019) Different Circulating Trace Amine Profiles in De Novo and Treated Parkinson's Disease Patients. *Scientific reports* 9: 6151

Devine MJ, Gwinn K, Singleton A, Hardy J (2011) Parkinson's disease and alpha-synuclein expression. *Mov Disord* 26: 2160-8

Dickson DW (2018) Neuropathology of Parkinson disease. *Parkinsonism Relat Disord* 46 Suppl 1: S30-S33

Erez A, DeBerardinis RJ (2015) Metabolic dysregulation in monogenic disorders and cancer - finding method in madness. *Nat Rev Cancer* 15: 440-8

Erez A, Nagamani SC, Lee B (2011a) Argininosuccinate lyase deficiency-argininosuccinic aciduria and beyond. *Am J Med Genet C Semin Med Genet* 157: 45-53

Erez A, Nagamani SC, Shchelochkov OA, Premkumar MH, Campeau PM, Chen Y, Garg HK, Li L, Mian A, Bertin TK, Black JO, Zeng H, Tang Y, Reddy AK, Summar M, O'Brien WE, Harrison DG, Mitch WE, Marini JC, Aschner JL et al. (2011b) Requirement of argininosuccinate lyase for systemic nitric oxide production. *Nat Med* 17: 1619-26

Galter D, Buervenich S, Carmine A, Anvret M, Olson L (2003) ALDH1 mRNA: presence in human dopamine neurons and decreases in substantia nigra in Parkinson's disease and in the ventral tegmental area in schizophrenia. *Neurobiol Dis* 14: 637-47

Giguere N, Burke Nanni S, Trudeau LE (2018) On Cell Loss and Selective Vulnerability of Neuronal Populations in Parkinson's Disease. *Front Neurol* 9: 455

Good PF, Hsu A, Werner P, Perl DP, Olanow CW (1998) Protein nitration in Parkinson's disease. *J Neuropathol Exp Neurol* 57: 338-42

Grenn FP, Kim JJ, Makarious MB, Iwaki H, Illarionova A, Brolin K, Kluss JH, Schumacher-Schuh AF, Leonard H, Faghri F, Billingsley K, Krohn L, Hall A, Diez-Fairen M, Perinan MT, Foo JN, Sandor C, Webber C, Fiske BK, Gibbs JR et al. (2020) The Parkinson's Disease Genome-Wide Association Study Locus Browser. *Mov Disord* 35: 2056-2067

Grunblatt E, Zehetmayer S, Jacob CP, Muller T, Jost WH, Riederer P (2010) Pilot study: peripheral biomarkers for diagnosing sporadic Parkinson's disease. *J Neural Transm (Vienna)* 117: 1387-93

Haeussler M, Zweig AS, Tyner C, Speir ML, Rosenbloom KR, Raney BJ, Lee CM, Lee BT, Hinrichs AS, Gonzalez JN, Gibson D, Diekhans M, Clawson H, Casper J, Barber GP, Haussler D, Kuhn RM, Kent WJ (2019) The UCSC Genome Browser database: 2019 update. *Nucleic Acids Res* 47: D853-D858

Harraz MM, Snyder SH (2015) Nitric Oxide-GAPDH Transcriptional Signaling Mediates Behavioral Actions of Cocaine. *CNS Neurol Disord Drug Targets* 14: 757-63

Hassani OK, Rymar VV, Nguyen KQ, Huo L, Cloutier JF, Miller FD, Sadikot AF (2020) The noradrenergic system is necessary for survival of vulnerable midbrain dopaminergic neurons: implications for development and Parkinson's disease. *Neurobiol Aging* 85: 22-37

Irwin DJ, Lee VM, Trojanowski JQ (2013) Parkinson's disease dementia: convergence of alpha-synuclein, tau and amyloid-beta pathologies. *Nat Rev Neurosci* 14: 626-36

Jimenez-Jimenez FJ, Alonso-Navarro H, Garcia-Martin E, Agundez JAG (2020) Cerebrospinal and blood levels of amino acids as potential biomarkers for Parkinson's disease: review and meta-analysis. *Eur J Neurol* 27: 2336-2347

Jimenez-Jimenez FJ, Alonso-Navarro H, Herrero MT, Garcia-Martin E, Agundez JA (2016) An Update on the Role of Nitric Oxide in the Neurodegenerative Processes of Parkinson's Disease. *Curr Med Chem* 23: 2666-2679

Jin Z, Kho J, Dawson B, Jiang MM, Chen-Evenson Y, Ali S, Burrage LC, Grover M, Palmer DJ, Turner DL, Ng P, Nagamani SC, Lee B (2020) Nitric oxide modulates bone anabolism through regulation of osteoblast glycolysis and differentiation. *J Clin Invest*

Kalia LV, Lang AE (2015) Parkinson's disease. *Lancet* 386: 896-912

Kho J, Tian X, Wong WT, Bertin T, Jiang MM, Chen S, Jin Z, Shchelochkov OA, Burrage LC, Reddy AK, Jiang H, Abo-Zahrah R, Ma S, Zhang P, Bissig KD, Kim JJ, Devaraj S, Rodney GG, Erez A, Bryan NS et al. (2018) Argininosuccinate Lyase Deficiency Causes an Endothelial-Dependent Form of Hypertension. *Am J Hum Genet* 103: 276-287

Kolker S, Garcia-Cazorla A, Valayannopoulos V, Lund AM, Burlina AB, Sykut-Cegielska J, Wijburg FA, Teles EL, Zeman J, Dionisi-Vici C, Baric I, Karall D, Augoustides-Savvopoulou P, Aksglaede L, Arnoux JB, Avram P, Baumgartner MR, Blasco-Alonso J, Chabrol B, Chakrapani A et al. (2015a) The phenotypic spectrum of organic acidurias and urea cycle disorders. Part 1: the initial presentation. *J Inherit Metab Dis* 38: 1041-57

Kolker S, Valayannopoulos V, Burlina AB, Sykut-Cegielska J, Wijburg FA, Teles EL, Zeman J, Dionisi-Vici C, Baric I, Karall D, Arnoux JB, Avram P, Baumgartner MR, Blasco-Alonso J, Boy SP, Rasmussen MB, Burgard P, Chabrol B, Chakrapani A, Chapman K et al. (2015b) The phenotypic spectrum of organic acidurias and urea cycle disorders. Part 2: the evolving clinical phenotype. *J Inherit Metab Dis* 38: 1059-74

Lerner S, Anderzhanova E, Verbitsky S, Eilam R, Kuperman Y, Tsoory M, Kuznetsov Y, Brandis A, Mehlman T, Mazkereth R, Neuropsychologists U, McCarter R, Segal M, Nagamani SCS, Chen A, Erez A (2019) ASL Metabolically Regulates Tyrosine Hydroxylase in the Nucleus Locus Coeruleus. *Cell Rep* 29: 2144-2153 e7

Liu G, Yu J, Ding J, Xie C, Sun L, Rudenko I, Zheng W, Sastry N, Luo J, Rudow G, Troncoso JC, Cai H (2014) Aldehyde dehydrogenase 1 defines and protects a nigrostriatal dopaminergic neuron subpopulation. *J Clin Invest* 124: 3032-46

Madisen L, Zwingman TA, Sunkin SM, Oh SW, Zariwala HA, Gu H, Ng LL, Palmiter RD, Hawrylycz MJ, Jones AR, Lein ES, Zeng H (2010) A robust and high-throughput Cre reporting and characterization system for the whole mouse brain. *Nat Neurosci* 13: 133-40

McDowell K, Chesselet MF (2012) Animal models of the non-motor features of Parkinson's disease. *Neurobiol Dis* 46: 597-606

Miller DB, O'Callaghan JP (2015) Biomarkers of Parkinson's disease: present and future. *Metabolism* 64: S40-6

Mittal S, Bjornevik K, Im DS, Flierl A, Dong X, Locascio JJ, Abo KM, Long E, Jin M, Xu B, Xiang YK, Rochet JC, Engeland A, Rizzu P, Heutink P, Bartels T, Selkoe DJ, Caldarone BJ, Glicksman MA, Khurana V et al. (2017) beta2-Adrenoreceptor is a regulator of the alpha-synuclein gene driving risk of Parkinson's disease. *Science* 357: 891-898

Mor DE, Daniels MJ, Ischiropoulos H (2019) The usual suspects, dopamine and alpha-synuclein, conspire to cause neurodegeneration. *Mov Disord* 34: 167-179

Mori M, Gotoh T (2004) Arginine metabolic enzymes, nitric oxide and infection. *J Nutr* 134: 2820S-2825S; discussion 2853S

Nagamani SC, Campeau PM, Shchelochkov OA, Premkumar MH, Guse K, Brunetti-Pierri N, Chen Y, Sun Q, Tang Y, Palmer D, Reddy AK, Li L, Slesnick TC, Feig DI, Caudle S, Harrison D, Salviati L, Marini JC, Bryan NS, Erez A et al. (2012) Nitric-oxide supplementation for treatment of long-term complications in argininosuccinic aciduria. *Am J Hum Genet* 90: 836-46

Nagamani SCS, Erez A, Lee B (1993) Argininosuccinate Lyase Deficiency. In *GeneReviews*, Pagon RA, Bird TD, Dolan CR, Stephens K, Adam MP (eds) Seattle (WA):

Nalls MA, Blauwendraat C, Vallerga CL, Heilbron K, Bandres-Ciga S, Chang D, Tan M, Kia DA, Noyce AJ, Xue A, Bras J, Young E, von Coelln R, Simon-Sanchez J, Schulte C, Sharma M, Krohn L, Pihlstrom L, Siitonen A, Iwaki H et al. (2019) Identification of novel risk loci, causal insights, and heritable risk for Parkinson's disease: a meta-analysis of genome-wide association studies. *Lancet Neurol* 18: 1091-1102

Neufeld-Cohen A, Tsoory MM, Evans AK, Getselter D, Gil S, Lowry CA, Vale WW, Chen A (2010) A triple urocortin knockout mouse model reveals an essential role for urocortins in stress recovery. *Proc Natl Acad Sci U S A* 107: 19020-5

Poulin JF, Zou J, Drouin-Ouellet J, Kim KY, Cicchetti F, Awatramani RB (2014) Defining midbrain dopaminergic neuron diversity by single-cell gene expression profiling. *Cell Rep* 9: 930-43

Premkumar MH, Sule G, Nagamani SC, Chakkalakal S, Nordin A, Jain M, Ruan MZ, Bertin T, Dawson B, Zhang J, Schady D, Bryan NS, Campeau PM, Erez A, Lee B (2014) Argininosuccinate lyase in enterocytes protects from development of necrotizing enterocolitis. *Am J Physiol Gastrointest Liver Physiol* 307: G347-54

Rommelfanger KS, Weinshenker D, Miller GW (2004) Reduced MPTP toxicity in noradrenaline transporter knockout mice. *J Neurochem* 91: 1116-24

Sade D, Shaham-Niv S, Arnon ZA, Tavassoly O, Gazit E (2018) Seeding of proteins into amyloid structures by metabolite assemblies may clarify certain unexplained epidemiological associations. *Open Biol* 8

Sara SJ (2009) The locus coeruleus and noradrenergic modulation of cognition. *Nat Rev Neurosci* 10: 211-23

Schapira AHV, Chaudhuri KR, Jenner P (2017) Non-motor features of Parkinson disease. *Nat Rev Neurosci* 18: 435-450

Sgobio C, Wu J, Zheng W, Chen X, Pan J, Salinas AG, Davis MI, Lovinger DM, Cai H (2017) Aldehyde dehydrogenase 1-positive nigrostriatal dopaminergic fibers exhibit distinct projection pattern and dopamine release dynamics at mouse dorsal striatum. *Sci Rep* 7: 5283

Shaham-Niv S, Adler-Abramovich L, Schnaider L, Gazit E (2015) Extension of the generic amyloid hypothesis to nonproteinaceous metabolite assemblies. *Sci Adv* 1: e1500137

Srinivasan J, Schmidt WJ (2003) Potentiation of parkinsonian symptoms by depletion of locus coeruleus noradrenaline in 6-hydroxydopamine-induced partial degeneration of substantia nigra in rats. *Eur J Neurosci* 17: 2586-92

Stettner N, Rosen C, Bernshtein B, Gur-Cohen S, Frug J, Silberman A, Sarver A, Carmel-Neiderman NN, Eilam R, Biton I, Pevsner-Fischer M, Zmora N, Brandis A, Bahar Halpern K, Mazkereth R, di Bernardo D, Brunetti-Pierri N, Premkumar MH, Dank G, Nagamani SCS et al. (2018) Induction of Nitric-Oxide Metabolism in Enterocytes Alleviates Colitis and Inflammation-Associated Colon Cancer. *Cell Rep* 23: 1962-1976

Tavassoly O, Sade D, Bera S, Shaham-Niv S, Vocadlo DJ, Gazit E (2018) Quinolinic Acid Amyloid-like Fibrillar Assemblies Seed alpha-Synuclein Aggregation. *J Mol Biol* 430: 3847-3862

Tuchman M, Lee B, Lichter-Konecki U, Summar ML, Yudkoff M, Cederbaum SD, Kerr DS, Diaz GA, Seashore MR, Lee HS, McCarter RJ, Krischer JP, Batshaw ML (2008) Cross-sectional multicenter study of patients with urea cycle disorders in the United States. *Mol Genet Metab* 94: 397-402

Waisbren SE, Gropman AL, Members of the Urea Cycle Disorders C, Batshaw ML (2016) Improving long term outcomes in urea cycle disorders-report from the Urea Cycle Disorders Consortium. *J Inherit Metab Dis* 39: 573-84

Wang XH, Lu G, Hu X, Tsang KS, Kwong WH, Wu FX, Meng HW, Jiang S, Liu SW, Ng HK, Poon WS (2012) Quantitative assessment of gait and neurochemical correlation in a classical murine model of Parkinson's disease. *BMC Neurosci* 13: 142

Wang Y, Sung CC, Chung KK (2017) Novel enhancement mechanism of tyrosine hydroxylase enzymatic activity by nitric oxide through S-nitrosylation. *Sci Rep* 7: 44154

Wise RA (2004) Dopamine, learning and motivation. *Nat Rev Neurosci* 5: 483-94

Wong YC, Krainc D (2017) alpha-synuclein toxicity in neurodegeneration: mechanism and therapeutic strategies. *Nat Med* 23: 1-13

Wu J, Kung J, Dong J, Chang L, Xie C, Habib A, Hawes S, Yang N, Chen V, Liu Z, Evans R, Liang B, Sun L, Ding J, Yu J, Saez-Atienzar S, Tang B, Khaliq Z, Lin DT, Le W et al. (2019) Distinct Connectivity and Functionality of Aldehyde Dehydrogenase 1a1-Positive Nigrostriatal Dopaminergic Neurons in Motor Learning. *Cell Rep* 28: 1167-1181 e7

Xia Y, Dawson VL, Dawson TM, Snyder SH, Zweier JL (1996) Nitric oxide synthase generates superoxide and nitric oxide in arginine-depleted cells leading to peroxynitrite-mediated cellular injury. *Proc Natl Acad Sci U S A* 93: 6770-4

Zaguri D, Kreiser T, Shaham-Niv S, Gazit E (2018) Antibodies towards Tyrosine Amyloid-Like Fibrils Allow Toxicity Modulation and Cellular Imaging of the Assemblies. *Molecules* 23